Final Draft
of the original manuscript:

Froend, M.; Fomin, F.; Riekehr, S.; Alvarez, P.; Zubiri, F.; Bauer, S.; Klusemann, B.; Kashaev, N.:

Fiber laser welding of dissimilar titanium (Ti-6Al-4V/cp-Ti) T-joints and their laser forming process for aircraft application

In: Optics and Laser Technology (2017) Elsevier

DOI: 10.1016/j.surfcoat.2017.05.055

Fiber laser welding of dissimilar Titanium (Ti-6Al-4V/ cp-Ti) T-joints and their laser forming process for aircraft application

Authors: M. Froend[1,2], F. Fomin[2], S. Riekehr[2], P. Alvarez[3], F. Zubiri[3], S. Bauer[4], B. Klusemann[1,2], N. Kashaev[2]

Affiliations:

[1]Leuphana University of Lueneburg, Institute of Product and Process Innovation, Volgershall 1, D-21339 Lueneburg, Germany

[2]Helmholtz-Zentrum Geesthacht, Institute of Materials Research, Materials Mechanics, Max-Planck-Strasse 1, 21052 Geesthacht, Germany;

[3]IK4-LORTEK, Technological Centre, Department of Joining Processes, Arranomendia Kalea 4a, Ordizia (Gipuzkoa), 20240 Spain

[4]Airbus Operations GmbH, Department of Future Industrial System, Airbus-Allee 1, 28199 Bremen, Germany

Corresponding author: M. Froend, Tel.: +49-4152-87-2558, E-mail: martin.froend@hzg.de.

Keywords: Fiber laser beam welding, laser forming, Ti-6Al-4V, cp-Ti, T-joint,

Highlights

- Fiber laser beam welding and straightening of cp-Ti-Ti-6Al-4V T-joints was achieved
- High sensitivity on shielding conditions and positioning of the laser was detected
- Straightening behaviors of cp-Ti sheets and cp-Ti-Ti-6Al-4V T-joints was analyzed

Abstract

The weldability of dissimilar T-joints between commercially pure titanium (cp-Ti) Grade 2 skin and Ti-6Al-4V Grade 5 stringer using a continuous wave 8 kW ytterbium fiber laser as well as the possibility of subsequent laser straightening process of these joints were investigated. Based on the industrial standards ISO 4578:2011 and AWS D17.1:200, the process development to compensate the inherent angular distortion after welding by laser heating with the same equipment as for welding was carried out. The obtained results were effectively transferred to a 6-stringer-demonstrator with a length up to 500 mm. To investigate the shape and morphology of the welding seam as well as to verify its freedom from defects using the defined process parameters, metallographic transverse cross-sections and X-Ray analysis were realized. In addition, the general behavior of the welding seam geometry and the bending behavior of the specimens for varied process parameters were elucidated. For the welding process special attention to the shielding conditions and also to the local and angular laser beam positioning was payed. To straighten the welded joints, laser straightening parameters inducing no microstructural changes were identified.

Keywords: Fiber laser beam welding, laser forming, Ti-6Al-4V, cp-Ti, T-joint

1. Introduction

The global air traffic volume dramatically increased over the last decades resulting in a large input of fuel resources. Therefore, the aircraft industry focuses on the development of aerodynamically optimized structures in order to achieve weight and fuel savings [1]. The use of laser beam welding (LBW) technique instead of conventional riveting joints is a promising approach in the direction of cost and weight reduction. The latter imposes additional needs for advanced materials which conform to the strict requirements of high load capacity and low density [2]. Taking into account their excellent mechanical properties and high corrosion resistance, titanium alloys are very promising for application in aerospace. Because of its high strength titanium is difficult to form and process in general. Several alloying elements significantly increase the strength but reduce the formability of titanium alloys [3], [4]. This is the main reason why commercially pure titanium (Grade 2) is mostly used for the outer skin material, whereas Ti-6Al-4V titanium alloy (Grade 5) is usually chosen as stiffening stringer material. This research deals with the investigation of the general feasibility to weld and straighten T-joint-connections between Ti-6Al-4V stringer and commercially pure titanium Grade 2 as skin of 0.8 mm thickness using an 8 kW ytterbium fiber laser. Welded connections conforming to ISO 4578:2011 and to the American standard AWS D 17.1:2001 were produced. Due to distortional effects induced by residual stresses after the LBW-process, a subsequent straightening of the components is needed. These distortional effects result from high temperature differences between the upper and the lower material layer, which is also known as the temperature gradient mechanism (TGM) during LBW of T-joints. Therefore, the feasibility of an adequate non-contact post-straightening process, using the same laser equipment as for the welding of the T-joint connection, was carried out. This laser induced straightening (LIS) process is based on the TGM and involves the post processing of the joint by a defocused laser beam. In the following the development of an optimal parameter set for the LBW-process of the above mentioned joints as well as its LIS-process parameter identification is addressed.

2. Laser forming mechanism

Due to the heat input during the welding process, plastic deformation of the material occurs. This takes place by the temperature difference between the upper and the lower side of the skin sheet. [5]. The gradient causes the development of inhomogeneously distributed inner residual stresses which lead to an angular distortion of the sheet material. The effect is shown in Figure 1. To reconstruct the formerly flat surface of the material, post-forming processes have to be conducted [6]. In this work a non-contact post-forming procedure was performed using the formerly mentioned temperature gradient mechanism (TGM) to straighten the sheet material. Therefore, the rear side of the workpiece was irradiated by a defocused laser of the same equipment as for the LBW-process to induce the TGM again and reverse welding induced distortions. This technique is very efficient for small material thicknesses due to relatively fast process and minimum energy needs [7]–[10]. Aim of the straightening process is to achieve a flat surface of the workpiece similar to the flatness before the LBW. The required laser power should be minimized in order to prevent the damage of the surface, oxidation and microstructural changes. Therefore the laser beam has to be defocused and the operating laser power has to be controlled precisely.

Equation 2.1 shows the beam diameter as a function of the focus diameter (d_f) in dependence on the ratio of the distance of the optical head to the specimens surface (z) and the so called Rayleigh length (z_r).

$$d(z) = d_f \sqrt{1 + \left(\frac{z}{z_r}\right)^2} \tag{2.1}$$

Using this effect it is possible to regulate the surface power density (E) affecting the workpiece surface which is expressed by the ratio of the laser power (P) and the irradiated area of the workpiece (A_f):

$$E = \frac{P}{A_f} = \frac{P}{\pi \frac{{d_f}^2}{4}}, \tag{2.2}$$

The line energy (L_E) is determined by the ratio of the laser power (P) and the scan velocity (v_s)

$$L_E = \frac{P}{v_s}. \tag{2.3}$$

These three equations are enough to adapt the parameters of the laser system in order to remove the welding induced angular distortion of the specimen.

The distortion after the welding process is the initial condition for straightening experiments as shown in Figure 2 a [11]. The use of the TGM to straighten the bended skin sheet is shown in Figure 2 b.

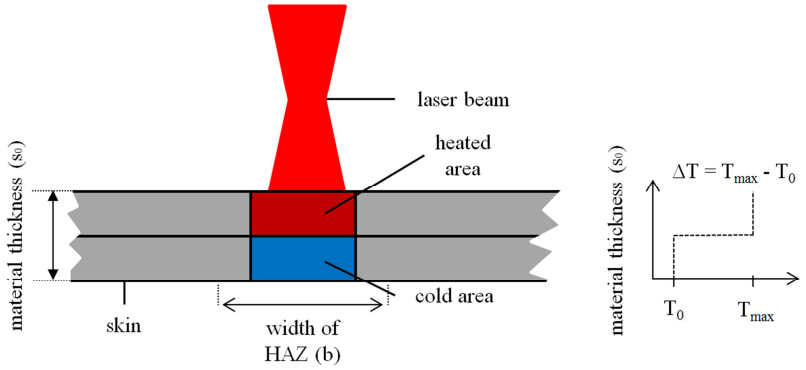

Figure 1: The TGM in a simplified two layer model according to [12]

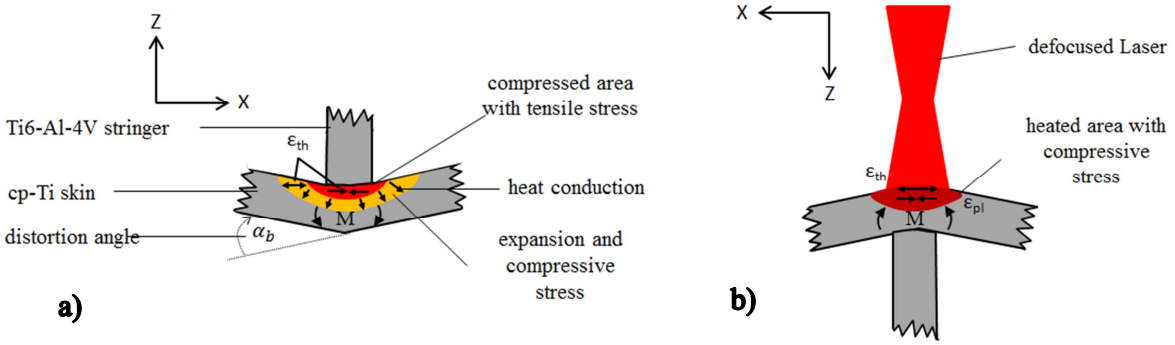

Figure 2: Distortion due to heat input during laser welding or laser straightening according to [11]

2.1 Existing predictive approach of angular distortion

A well-established approach to quantitatively predict the bending angle caused by the TGM is the analytical model of Vollertsen [13]–[15], which is based on a simple two-layer model shown in Figure 1. The bending angle (α_b) of the workpiece is defined as

$$\alpha_b = \frac{3b\,\alpha_{th}\,\Delta T}{2s_0} \tag{2.4}$$

where (b) is the width of the heat affected zone (HAZ), (α_{th}) the thermal expansion coefficient of the material, (s_0) the thickness of the workpiece and (ΔT) the temperature difference:

$$\Delta T = T_{max} - T_0 \tag{2.5}$$

which is a function of the absorption coefficient (A), the laser power, scan velocity, specific heat capacity (C_p), the width of the HAZ, the sheet thickness and its density (ρ) as given by equation

$$\Delta T = \frac{2\,A\,P}{v_s\,C_p\,b\,s_0\,\rho}\,. \tag{2.6}$$

As shown in [16] and [17] for larger geometries a size-effect occurs and increases the bending angle. The resulting bending angle, including size effects, can be analytically expressed by

$$\alpha_b = \left(1 - \frac{1}{3\,n}\right)\frac{2\,b}{s_0}\,\alpha_{th}\,\Delta T \tag{2.7}$$

The sheet is divided in n segments which are all assumed to behave in a uniform bending along the segments. The length of each segment is L/n and has to be determined. The value of n is related to the extent of the plastically deformed zone and predicted using a temperature model which assumes all thermal expansions to be fully converted into plastic deformation. The critical amount of line energy which has to be reached to achieve plastic deformation is shown in Equation 2.8

$$\frac{L}{n} = 3\,E - 17.5 \tag{2.8}$$

3. Experimental

3.1 Materials and process parameters

Table 1: Main properties of the laser equipment

Parameter	symbol	value	unit
Maximum power	P	8	kW
Collimation lens	L_C	120	mm
Focal lens	f	300	mm
Process fibre diameter	D	400	µm
Focal spot diameter	d_f	500	mm
Center wavelength	λ	1070	nm
Divergence half-angle	$\frac{\theta}{2}$	58.9	mrad
Beam parameter product	BPP	7.4	mm · mrad
Beam quality factor	M^2	22	-
Rayleigh length	z_r	8.5	mm

The main characteristics of the laser and the parameters of the focused beam are shown in Table 1. The welding and straightening equipment consisted of an 8 kW continuous wave ytterbium fibre laser YLS-8000-S2-Y12 (IPG Photonics Corporation) integrated with an optical head YW52 Precitec mounted on a 6-axis KUKA KR30HA industrial robot. For the welding and straightening experiments the α+β titanium alloy Ti-6Al-4V (Grade 5, AIMS03-18-004) as stringer material and commercially pure titanium (cp-Ti, Grade 2, AIMS03-18-002) as skin material were used. Standard chemical compositions of the materials as well as their mechanical characteristics are given in Table 2 and Table 3. The thickness of the sheets was 0.8 mm. The material was cut to a geometry shown in Figure 3 a and welded perpendicular to the rolling direction of the sheets.

For the LBW-process, the stringer was clamped and pressed to the skin material in order to achieve a zero gap. Before the welding, the edges of the specimens were milled, ground and then cleaned. Due to the high reactivity of titanium with oxygen and nitrogen which reduce the weld ductility and are deleterious to the overall weld performance, a local argon shielding device was mounted to the optical head. Furthermore, the skin material was clamped on a backing plate, having an argon filled gap which also provided shielding from underneath. The clamping as well as the shielding conditions are visualized in Figure 3. The used process parameters as well as the optical parameters which could be determined are given in Table 4 for LBW and in Table 5 for LIS.

Table 2: Chemical composition of Ti-6Al-4V and cp-Ti (wt.-%) [3], [4]

	Fe [%]	**O [%]**	**N [%]**	**C [%]**	**H [%]**	**Al [%]**	**V [%]**	**others individual [%]**	**others together [%]**	**Ti**
	min	**min**	**min**	**min**	**min**	**min**	**min**			
	max	**max**	**max**	**max**	**max**	**max**	**max**			
cp-Ti	-	-	-	-	-	-	-	-	-	Balance
	0.20	0.18	0.05	0.06	0.013	-	-	0.10	0.40	
Ti-6Al-4V	-	-	-	-	-	5.50	3.50	-	-	Balance
	0.30	0.20	0.05	0.08	0.015	6.75	4.50	0.10	0.40	

Table 3: Mechanical properties of Ti-6Al-4V and cp-Ti [18], [19]

	symbol	**unit**	**Ti-6Al-4V**	**cp-Ti**
desity	ρ	$\frac{kg}{m^3}$	4430	4500
melting temperature	T_M	K	1660	1660
thermal expansion coefficient	α_{th}	$\frac{1}{K}$	9.3	9
thermal conductivity	κ	$\frac{W}{m * K}$	7.1	22.6
specific heat capacity	C_P	$\frac{J}{kg * K}$	560	523
yield strength	σ_Y	MPa	940	398
tensile strength	R_m	MPa	1076	430

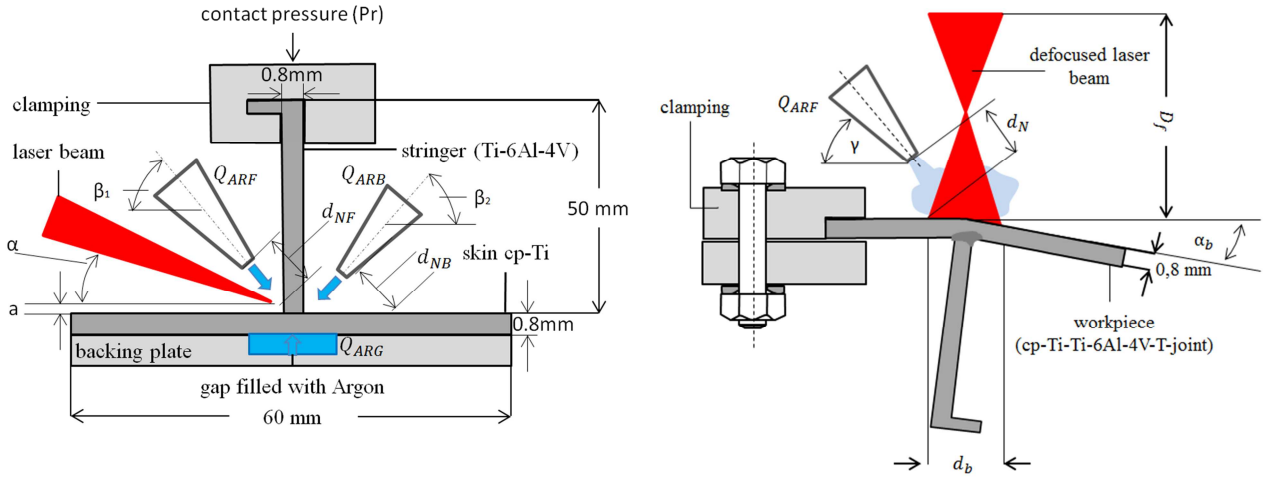

Figure 3: Shielding and clamping conditions during welding (a) and straightening (b) with an identification of process parameters of big influence

2.2 Metallographic and X-ray analysis

For metallographic investigations transverse cross-sections from the middle section of the weld were cut. They were mounted, ground and polished using an oxide polishing suspension compound (OPS). Microstructural observations were performed using an inverted optical microscopy (OM) Leica DMI 5000M. Prior to light microscopy, the specimens were etched by Kroll's reagent (3 % HF, 6 % HNO3, 91 % distilled water) for 30 s to reveal the microstructural features. The metallographic investigation was used to define the quality of the root fusion conditions. In this context the characterization of the HAZ depth in order to analyze its influence to the TGM was also studied.

In case of full stringer/skin connection, sufficient penetration in the skin and acceptable depth of the HAZ, an X-ray analysis was conducted in order to detect inner inhomogeneities like porosity in the welded seam. This analysis was performed by a DIN EN ISO 17636-1:2013-05-certified specialist using an Isovolt 320/13 X-ray tube, and incidence angle of 42°, a distance between the radiation source and the seam of 800 mm, a tube electricity of 4.2 mA and an effective focal spot of 1.5 x 1.5 mm.

3. Results and discussion

3.1 Morphology of the welding seams

The most important welding parameters were identified and are shown in Figure 3. Additional to these parameters the welding speed and the laser spot diameter is varied. Since the LBW-process is very sensitive to the energy input regarding the penetration of the welded parts [14] it is important to define a beam incidence angle with respect to the skin plane. In this context the identified parameter set 1 (see Table 4) with an incidence angle of 15° while welding directly in the intersection point between stringer and skin surfaces (a = 0 mm) is worked out. The welding speed during the LBW-process defines the time the workpiece is exposed to the laser radiation. In [13] and [14] is shown, that the porosity increased at low welding speeds. The latter and the need to use high welding speeds from a commercial point of view imply it´s maximization. Due to the restrictions imposed by commercially available seam tracking systems needed for the control of the LBW-process, the welding speed was limited and fixed at 3.5 m/min. As seen from Equations (2.1) - (**2.3**), the laser power required to keep the

energy density constant increases with increasing defocusing distance. Therefore all the LBW-processes were carried out in focal position to minimize the irradiated area of the workpiece as well as to work with a high degree of efficiency. In addition to that, the increased spot size would have been negative on the distortion due to the increased HAZ. Using these parameters the necessary laser power was defined to 725 W ± 3 % in order to get fully penetrated welds with a low HAZ depth in the skin material as well as an underfill depth of about 4 % which conforms to ISO 4578:2011 and AWS D17.1:2001 requirements. Taking into account the real shape of the stringers and the difficult access of the optical head to the required position in a manufacturing process at the subcomponent level, the incidence angle was increased to 25°. As can be seen in Figure 4 b, increasing the incidence angle from 15˚ to 25˚ and keeping all other parameters constant, the heat flow into the skin increases significantly. As a result, the skin was burnt through and unacceptable underfills appeared in the stringer material as well as in the skin. The reduction of the incidence angle position relatively to the skin also leads to an increased reflection of the beam from the skin surface back into the stringer and additionally increased the underfills in the stringer. With an increased incidence angle the joints were not fully penetrated even with a high laser power of 800 W (see Figure 4b). To eliminate an excessive heat input into the skin due to the higher incidence angle, the laser power should be restricted to less than 750 W. Only in this parameter window the skin is not burnt through. However, with such low power it is not possible to achieve a sufficient penetration (as shown in Figure 4 b). The latter implies that it is not possible to obtain fully penetrated T-joints without burning through the skin with a = 0 and α = 25˚. Therefore, the distance between the skin surface relatively to the irradiation point as well as the laser energy had to be adjusted. Figure 5 illustrates transverse cross sections of the welding seams welded with various laser powers and incidence positions for a focused beam at an incidence angle of 25° and at a welding speed of 3.5 m/min. It can be seen that there is a general dependence between the offset of the laser spot position and the power parameters, influencing the seam quality as well. A high sensitivity of the LBW-process regarding the power, incidence angle and position of the laser beam was found while processing these thin materials. An incidence position deviation of 0.1 - 0.2 mm significantly affects the quality of the seam and lead to welding seams not complying with the requirements. It should also be pointed out that increasing the power leads to an increase in the depth of the underfill but also improves the skin-stringer connection. The reduction of the incidence position of the laser beam increases the depth of the heat affected zone into the skin material but leads to a not welded stringer as shown in Figure 4 b and 5. It was not possible to achieve full penetration with the incidence position of a < 0.2 mm. If the incidence position is higher than 0.4 mm the energy of the laser is absorbed by the stringer leading to almost no connection between skin and stringer.

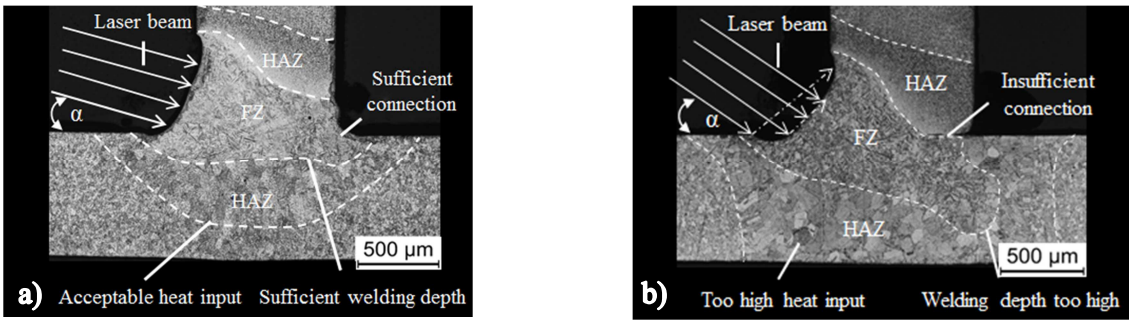

Figure 4: Differences of the seam morphology due to a different incidence angle 15° (a) and 25° (b)

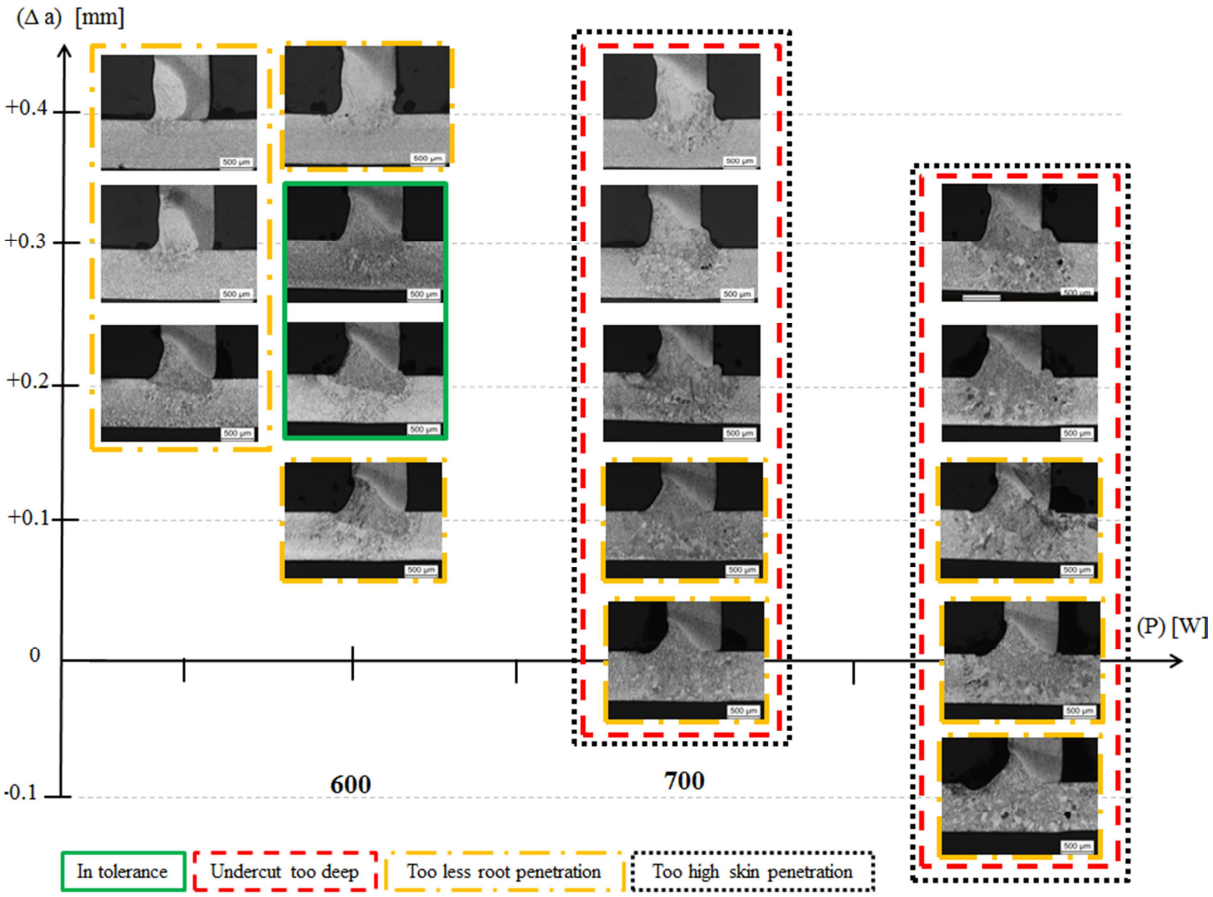

Figure 5: Metallographic visualization of the offset-power-ratio with respect to the seam morphology

3.2 Shielding conditions

Due to the high reactivity of the material with atmospheric gases, special attention has to be payed to the shielding conditions. By visual inspection it could be detected that stripes of discoloration with a width of approximately 4 mm appear on all sides of the fusion zone (FZ) after welding without shielding. This appears in consequence of the built oxide layer due to a reaction of the titanium with atmospheric gases. Taking the relatively small thickness of the specimens into account, it is evident that the not irradiated bottom side of the skin was heated up to a temperature where reactions with the atmosphere became possible. Therefore, the shielding gas has to be provided from the irradiated side of the stringer and skin material as well as from their rear side while LBW. During the LBW-process the irradiated material melts so that the flow rate of the shielding gas has to be defined as low as possible, in order to protect the liquid material from turbulences caused by too high gas pressure and solidified material from discoloration. For the LIS-process the energy density has to be much lower than for LBW in order not to melt the surface. Consequently, the temperature of the material surface is much lower and shielding has to be provided solely on the irradiated surface of the specimen. Table 4 lists three identified welding parameter sets. It was found that for an incident angle of 15°, a laser power of 700 – 750 W in connection with a welding speed of 3.5 m/min and an offset of 0 mm using a focused beam have to be used to get full penetrated welds as visualized in Figure 4 a. For a high incident angle of 25° the laser power could be reduced to 600 – 650 W in connection with an offset of 0.2 or 0.3 mm. Figures 6 a-c visualize the metallographic seam morphology using the identified parameter sets 1-3.

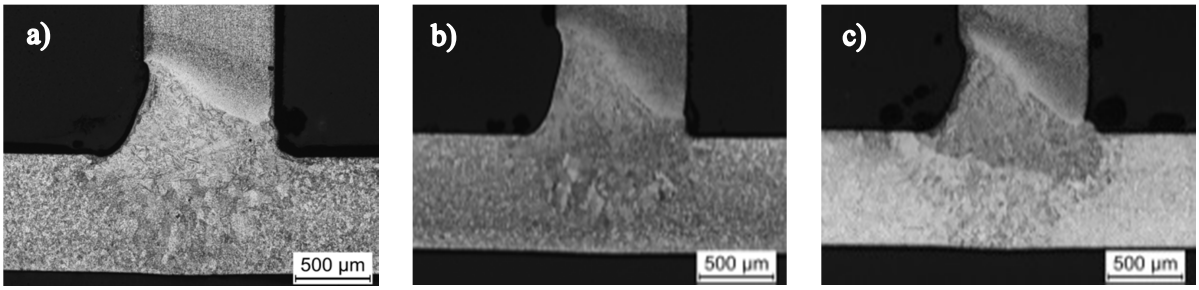

Figure 6: Metallographic seam morphology of defined best parameter sets

Table 4: Experimental parameter used for LBW

parameters	symbol	unit	parameter variation	identified parameter set 1	identified parameter set 2	identified parameter set 3
Beam angle	α	°	15, 25	15	25	25
Laser Power	P	W	500, 550, 600, 650, 700, 750, 800	700 - 750	600 - 650	600 - 650
Incident position/ offset	a	mm	0, 0.1, 0.2, 0.3, 0.4	0	0.2	0.3
Advance speed	v_s	m/min	3, 3.5, 4	3.5	3.5	3.5
Focus	F	mm	0	0	0	0
Contact load	P_r	kg	5, 6, 7, 8, 9, 10, 11, 12, 13	9	9	9
Argon flow beam side	Q_{ArF}	l/min	3, 4, 5, 6, 7, 8, 9, 10, 11	5	5	5
Argon flow back side	Q_{ArB}	l/min	3, 4, 5, 6, 7, 8, 9	6	6	6
Argon flow in the gap	Q_{ArG}	l/min	3, 4, 5, 6, 7, 8, 9	7	7	7
Front Nozzle Angle	β_1	°	30, 45, 60	45	45	45
Back Nozzle Angle	β_2	°	15, 20, 25, 30	20	20	20
Distance Front Nozzle to specimen	d_{NF}	mm	13,12,11,10,9,8,7, 6	10	10	10
Distance back Nozzle to specimen	d_{NB}	mm	7, 6, 5, 4, 3	3	3	3

3.3 LIS efficiency

To straighten the material using the TGM, investigations of the general distortion behaviour of cp-Ti were carried out. Preliminary tests were conducted on the specimens from cp-Ti without stringers. Different laser powers and scan velocities were used to analyze the dependence of the bending angle on the line energy. Due to the increased stiffness of the skin plate after the LBW-process, a different LIS efficiency was expected for the LBW joints compared to the skin material. The general behaviour of the cp-Ti sheets, cp-Ti-Ti-6Al-4V T-joints as well as the theoretical predictions from Equation 2.7 are shown in Figure 7. It was found that the welded T-joints showed a reduced bending behavior relatively to the cp-Ti sheets. As described in [20] the FZ of the LBW joints exhibit higher strength and lower ductility compared to the base metal. The reason for the increased strength is the high cooling rate which leads to microstructural changes within the FZ. The inner stresses which were induced while LIS do not reach the magnitude to distort the welded material like not welded

cp-Ti sheets using the same parameters. The distortional peak for not welded skin was reached using the line energy of 3.5 kJ/m to 3.2° ± 0.5° using a laser spot diameter of 4.5 mm. For cp-Ti-Ti-6Al-4V-T-joints the peak was shifted to 1.4° using the line energy of 1.8 kJ/m. Additionally, it was worked out that the general bending behavior reduced for T-joints. This is explained by the hardened material after welding. The theoretical prediction using Equation (2.4) correlates only for line energies from 1.3 kJ/m to 2.2 kJ/m in case of cp-Ti sheet material. In case of multipass LIS-process theoretical predictions of cp-Ti sheet material correlate very well with the calculated behaviour as displayed in Figure 7 b. Therefor a line energy of 1.5 kJ/m was used which was the necessary amount to straighten the welded specimens to a flatness of 80%. The maximum discrepancy of 5.76° between experimental results and calculated values appeared at a level of 10 passes, in case of the LBW T-joint the maximum discrepancy of 29.34° occurred for 30 passes. In general, it was shown that the bending behaviour of multipass LIS-processes is not linear and the efficiency decreases with increasing number of passes. As found in [16], this effect is based on the increasing material thickness of the bending edge after multiple irradiations.

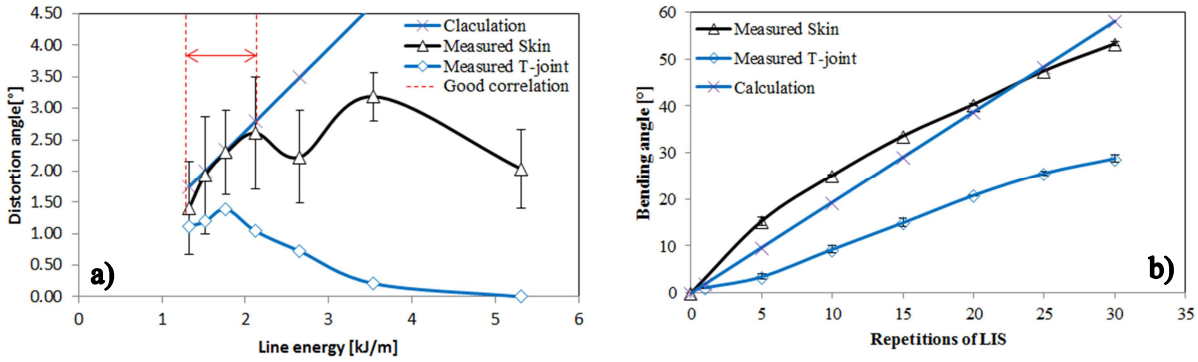

Figure 7: Distortional behaviour of cp-Ti-sheets and Ti-6Al-4V-cp-Ti-T-joints single (a) and multiple LIS (b)

Using the determined LIS parameter set shown in Table 5 a six-stringer demonstrator could be straightened after the LBW by applying LIS on the reverse of each T-joint. The identified parameter set fulfilled the general requirements to straighten the material without melting the surface using the same equipment and low power in connection with a maximum velocity of 3.5 m/min. An average bending angle of 1.0°± 0.28° was measured and could be reduced to 0.2° ± 0.14° after the straightening, which implies an efficiency of 80 %. This LIS-process corrects the occurred distortion to an almost flat surface. The angular dimensions of the manufactured demonstrator are shown in Figure 9. For a general prediction of the needed specimen dimension to show occurring size-effects Equation (2.7) and 2.8 were used. The calculations showed a predicted bending angle of 3° for a 50 mm long workpiece and an increasing size effect to 3.71° for a 4000 mm long panel. This behavior is also shown in Figure 8 a. Measured results showed an average bending angle of 2.2° for 50 mm long specimens and an average bending angle of 1° in case of a 100 mm long demonstrator with six-stringers. This result underlines the necessity of ongoing future work in this field of research. To achieve a precise prediction of the occurring bending behavior of cp-Ti-Ti-6Al-4V-Tjoints further experimental as well as advanced numerical modeling strategies have to be pursued.

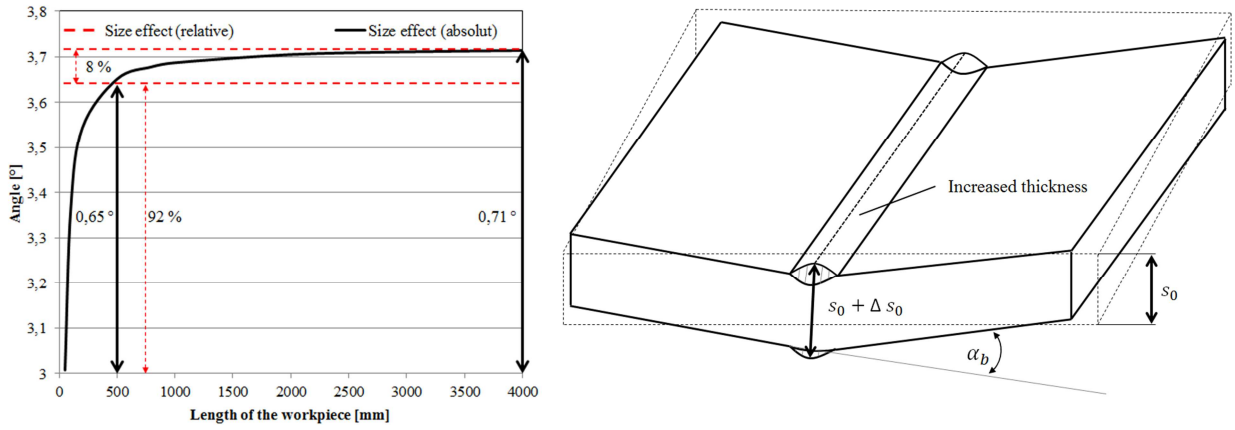

Figure 8: Estimation of the size-effect (a) and thickness increasing effects in the bending edge (b)

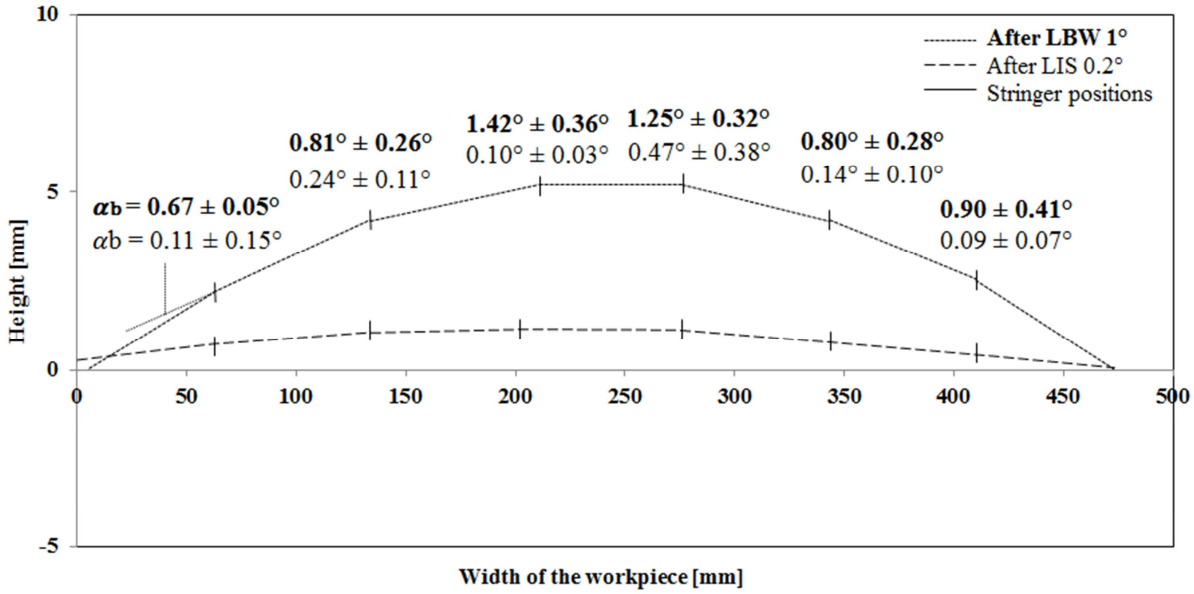

Figure 9: Distortions over the width of the workpiece after LBW and LIS

Table 5: Experimental parameter used for LIS

parameters	symbol	unit	parameter variation	identified parameter set
Laser power	P	W	600, 900, 1200	900
Beam angle	α	°	-	90
Defocusing	D_f	mm	40, 60, 80, 100, 120	80
Advance speed	v_s	m/min	0.5, 1, 1.5, 2, 2.5, 3, 3.5, 4	3.5
Argon flow beam side	Q_{ARF}	l/min	10, 15, 20, 25	20
Nozzle Angle	γ	°	15, 20, 25, 30	20
Distance Nozzle to specimen	d_{NS}	mm	4, 3, 2, 1	1
Beam diameter	d_b	mm	2, 3.2, 4.5, 5.5, 7	4.5

4. Conclusion

Dissimilar T-joints between cp-Ti skin and Ti-6Al-4V stringer were laser beam welded to investigate the influence of welding parameters on the weld quality, shape, distortion and defects. 13 process parameters were identified to have a strong influence on the weld quality. Special supporting measures need to be taken in order to provide sufficient shielding of the molten material from atmospheric gases. Local shielding with nozzles mounted on the optical head led to the desired results. The challenging problem to protect the bottom side of the skin was solved by using a clamping device with an argon filled gap under the skin. The LBW parameters were optimized for two different incidence angles, namely 15° and 25°. With a lower incidence angle it was possible to weld with zero offset from the skin, i.e. in the intersection point of skin and stringer surfaces. In contrast, welding with an incidence angle of 25° requires the laser spot to be positioned with 0.2 - 0.3 mm offset. The joints obtained with a laser power of 650 W and welding speed of 3.5 m/min showed full penetration along the whole length of the seam and acceptable depth of undercuts. Incomplete penetration was the main problem at low laser power, whereas, undercuts and burnt through skin were the main defects at high laser power. Large coupons up to 500 mm length with 2 stringers were welded with optimal parameter sets in order to verify the size effect. Stable fully penetrated welds were obtained with low values of undercuts depths and no discoloration conforming to European as well as American specifications. The heat induced distortion angle due to the LBW of the cp-Ti and Ti-6Al-4V, using the optimum parameter set, was in average 1.0° ± 0.28° in case of a 100 mm long welding seam.

It needs to be pointed out that for the LIS the laser system has to be defocused to achieve a focus diameter which is large enough to irradiate the necessary width of the backside of the skin. Using the described equipment a defocusing distance of 80 mm with a laser power of 900 W and a scan velocity of 3.5 m/min, a material straightening to 0.2° ± 0.14° was achieved. Furthermore, the developed shielding device with an argon flow of 20 l/min was found to be sufficient to protect the material from discoloration. The defined parameter set is proven to straighten the welded T-joint-connections without melting or damaging the surface. During the investigations of the straightening behavior of the manufactured joints it was also observed that there is a strong sensitivity of the process to the line energy, which has to be well adjusted for the highest efficiency. The straightening effect in the multipass LIS is not linear. The effect decreases due to material hardening, increasing thickness of the bending edge diameter and the changes in surface properties. The distortion effect is influenced by the size of the workpiece so that the distortion increases with increasing length.

Acknowledgements

The authors gratefully acknowledge the financial support of the European Union (Clean Sky 2 EU-JTI Platform) under the thematic call JTI-CS2-2014-CFP01-LPA-01-03 “Development of advanced laser based technologies for the manufacturing of titanium HLFC structures / DELASTI” (grant agreement no: 687088).

Additionally the authors would like to thank Mr. R. Dinse and Mr. F. Dorn from Helmholtz-Zentrum Geesthacht for their valuable technical support.

5. References

[1] D. Dittrich, J. Standfuss, J. Liebscher, B. Brenner, and E. Beyer, "Laser Beam Welding of Hard to Weld Al Alloys for a Regional Aircraft Fuselage Design – First Results" *Physics Procedia*, vol. 12, pp. 113–122, 2011.

[2] J. Enz, H. Iwan, S. Riekehr, V. Ventzke, and N. Kashaev, "Fracture Behavior of a Laser Beam Welded High-strength Al-Zn Alloy," *Procedia Materials Science*, vol. 3, pp. 1828–1833, 2014.

[3] A. D. McNaught and A. Wilkinson, *the "Gold Book"* Blackwell Scientific Publications, Oxford, 1997.

[4] Dt. Inst. für Normung, *DIN 17850:1990-11 Titan, chemische Zusammensetzung*.

[5] R. Pfeiffer, *Richten und Umformen mit der Flamme*. Düsseldorf: DVS- Verlag, 1989.

[6] A. Peiter, R. Gebhardt, and D. Seel, *Verformung und Eigenspannung beim Flammrichten. Bänder Bleche Rohre 2*, 1983.

[7] K. G. Watkins *et al.*, "Laser Forming of Aerospace Alloys" *Society of Automotive Engineers*, vol. 1, 2001.

[8] T. Hennige, "Laser forming of spatially curved parts" *Proceedings of the LANE*, pp. 409–420, 1997.

[9] J. Magee, K. G. Watkins, and T. Hennige, "Symmetrical laser forming" *Proceedings of ICALEO*, pp. 77–86, 1999.

[10] K. Masubuchi, "Studies at M. I. T. related to applications of laser technologies to metal fabrication," *Proceedings of the LANE, Nagaoka*, pp. 939–946, 1992.

[11] F. Vollertsen, *Laserstrahlumformen - Lasergestützte Formgebun: Verfahren, Mechanismen, Modellierung*. Bamberg: Meisenbach, 1996.

[12] H. Jung, "A Study on Laser Forming Processes with Finite Element Analysis" April, 2006.

[13] F. Vollertsen, "An analytical model for laser bending" *Lasers in Engineering 2*, pp. 261–276, 1994.

[14] F. Vollertsen, "Mechanisms and models for laser forming" *Proceedings of the LANE*, pp. 345–359, 1994.

[15] F. Vollertsen and M. Rodle, "Model for the temperature gradient mechanism of laser bending" *Proceedings of the LANE*, pp. 371–378, 1994.

[16] Y. Shi, Y. Liu, P. Yi, and J. Hu, "Effect of different heating methods on deformation of metal plate under upsetting mechanism in laser forming" *Optics and Laser Technology*, vol. 44, no. 2, pp. 486–491, 2012.

[17] P. Cheng, Y. L. Yao, C. Liu, D. Pratt, and Y. Fan, "On laser forming of sheet metal," Department of Mechanical Engineering Columbia University, New York, NY 10027, vol. 32, pp. 439–446, 2004.

[18] M. Peters, C. Leyens, and J. Kumpfert, *Titan und Titanlegierungen.* DGM Informationsgesellschaft mbH, 1996.

[19] ThyssenKrupp, "Titan Grade 5," 2016. [Online]. Available: http://www.thyssenkrupp.ch/documents/Titan_Grade_5.pdf.

[20] N. Kashaev, V. Ventzke, V. Fomichev, F. Fomin, and S. Riekehr, "Effect of Nd : YAG

laser beam welding on weld morphology and mechanical properties of Ti – 6Al – 4V butt joints and T-joints," *Optics and Lasers in Engineering*, vol. 86, pp. 172–180, 2016.

[21] F. Fomin et al., "Effect of Microstructure Transformations on Fatigue Properties of Laser Beam Welded Ti-6Al-4V Butt Joints Subjected to Postweld Heat Treatment", "Study of Grain Boundary Character", 2016.